

Hybrid-bias and displacement emulators for field-level modelling of galaxy clustering in real and redshift space

Marcos Pellejero Ibañez,^{1,2}★ Raul E. Angulo,^{1,3}† Drew Jamieson⁴, and Yin Li^{5,6,7}

¹ Donostia International Physics Centre, Paseo Manuel de Lardizabal 4, 20018 Donostia-San Sebastian, Spain.

² Institute for Astronomy, University of Edinburgh, Royal Observatory, Blackford Hill, Edinburgh, EH9 3HJ, UK

³ IKERBASQUE, Basque Foundation for Science, 48013, Bilbao, Spain.

⁴ Max-Planck-Institut für Astrophysik, Karl-Schwarzschild-Straße 1, 85748 Garching, Germany.

⁵ Department of Mathematics and Theory, Peng Cheng Laboratory, Shenzhen, Guangdong 518066, China.

⁶ Center for Computational Mathematics, Flatiron Institute, New York, New York 10010, USA.

⁷ Center for Computational Astrophysics, Flatiron Institute, New York, New York 10010, USA.

Accepted XXX. Received YYY; in original form ZZZ

ABSTRACT

Recently, hybrid bias expansions have emerged as a powerful approach to modelling the way in which galaxies are distributed in the Universe. Similarly, field-level emulators have recently become possible thanks to advances in machine learning and N -body simulations. In this paper we explore whether both techniques can be combined to provide a field-level model for the clustering of galaxies in real and redshift space. Specifically, here we will demonstrate that field-level emulators are able to accurately predict all the operators of a 2nd-order hybrid bias expansion. The precision achieved in real and redshift space is similar to that obtained for the nonlinear matter power spectrum. This translates to roughly 1-2% precision for the power spectrum of a BOSS and a Euclid-like galaxy sample up to $k \sim 0.6h \text{ Mpc}^{-1}$. Remarkably, this combined approach also delivers precise predictions for field-level galaxy statistics. Despite all these promising results, we detect several areas where further improvements are required. Therefore, this work serves as a road-map for the developments required for a more complete exploitation of upcoming large-scale structure surveys.

Key words: cosmology: theory – large-scale structure of Universe

1 INTRODUCTION

The spatial distribution of galaxies encodes valuable information about the Universe. By examining the statistical features of this distribution we can infer precise details of the composition of the Universe, its expansion history, the formation history of cosmic structure, and the underlying physical laws governing these phenomena. Numerous observational surveys are poised to generate detailed 3-dimensional maps of the galaxies distribution. These maps will provide tight constraints on cosmology and gravitational physics, and could lead to a measurement of the neutrino mass and the discovery of new physics (e.g. Euclid, Laureijs et al. 2011 and Amendola et al. 2018, and DESI, Levi et al. 2013).

Extracting the maximum amount of information from these upcoming large-scale structure (LSS) surveys is an active field of research. Traditionally, the two point statistics (power spectrum and correlation function) have been the primary basis for cosmological inference (see e.g. Cole et al. 2005; Blake et al. 2010; Beutler et al. 2017; Pellejero-Ibanez et al. 2017). However, since the galaxy field and the underlying dark matter are highly non-Gaussian, a large

amount of information lies in higher order statistics. For instance, constraints from the BOSS survey tighten by 15–20% when the bispectrum is jointly analysed along with the power spectrum (see e.g. Philcox & Ivanov 2022 and Ivanov et al. 2023). Recently, a plethora of additional summary statistics have been proposed, including k-nearest-neighbours (kNNs, Banerjee & Abel 2021), cosmic voids (Pisani et al. 2019; Moresco et al. 2022), wavelet scattering transforms (Cheng et al. 2020; Valogiannis & Dvorkin 2022a,b), line-correlation functions (Eggemeier et al. 2015), and artificial intelligence algorithms (Hahn et al. 2023). Ultimately, the only way to guarantee that the full amount of information is extracted from observational data is to model the data at the field level, utilising the information from every single observed resolution unit – a topic that has recently attracted a lot of attention from the community (see e.g. Kostić et al. 2022; Stadler et al. 2023; Porqueres et al. 2023; Boruah & Rozo 2023).

A common challenge for all analysis methods, regardless of whether they use field-level or summary statistics, is to guarantee the robustness of the corresponding theoretical model. Although numerical simulations of galaxy formation have advanced enormously over the last decade, they make assumptions and simplifications about galaxy formation physics, which might not be valid in the real Universe at the precision of LSS surveys. Empirical models (such as

★ E-mail: mpelleje@roe.ac.uk (MPI)

† E-mail: reangulo@dipc.org (REA)

Halo Occupation Distribution and/or SubHalo Abundance Matching) offer a more agnostic approach, but they still rely on correctly modelling the underlying processes, which cannot be formally guaranteed. Conversely, perturbative descriptions of biased tracers offer robustness, in the sense that these should be valid regardless of the details of galaxy formation as long as certain symmetries are present. Unfortunately, perturbation theory is valid only on very large scales, which implies that a large amount of information would be discarded in data analyses.

Ideally, we would like to leverage the advantages of both the accurate N -body model of nonlinear gravitational clustering and the perturbative description of uncertain bias relations. This can be achieved by combining a Lagrangian-space bias expansion with displacement and velocity fields measured from N -body simulations. Using N -body to transform from Lagrangian to Eulerian coordinates extends the range of validity of the perturbative expansion down to mildly nonlinear scales. Recent work by Modi et al. (2020) and Pellejero Ibañez et al. (2022) demonstrated the effectiveness of this approach in accurately modelling galaxy clustering down to $k = 0.6h \text{ Mpc}^{-1}$. These authors also employed this hybrid model in real and redshift space to construct power spectra emulators (Zennaro et al. 2021; Kokron et al. 2021; Pellejero Ibañez et al. 2023), achieving significant gains for these summary statistics. Field-level analysis, however, requires generating full 3-dimensional galaxy fields, which cannot be obtained from summary statistics emulators.

Exploiting the benefits of a hybrid bias approach at the field level requires making faster predictions for the nonlinear displacement field than can be directly obtained from N -body simulations. Speeding up this prediction typically sacrifices accuracy, such as under n^{th} order Lagrangian Perturbation theory (LPT) with or without suitable enhancements (see Desjacques et al. 2018 for a review), or through approximate, low resolution N -body solvers (see e.g. Feng et al. 2016; Tassev et al. 2013). Another approach is to use deep learning models to emulate the N -body evolution at the field level, which can greatly accelerate the prediction while retaining N -body accuracy on relevant scales (see e.g. He et al. 2019; Alves de Oliveira et al. 2020; Kaushal et al. 2022; Jamieson et al. 2022).

The basic idea behind field-level emulators is to employ convolutional neural networks to learn the mapping between a fully nonlinear displacement field and an approximation of this field predicted by a fast method. The versatility of convolutional neural networks enables a broad range of applications, including super-resolution simulation (Li et al. 2021; Ni et al. 2021; Zhang et al. 2023) and error correction for approximate N -body solvers (Kaushal et al. 2022; Jamieson et al. 2022). In this paper we implement the state-of-the-art field-level emulator map2map¹ from Jamieson et al. 2022 in our hybrid bias expansion model. This emulator extends the capabilities of neural network models by incorporating dependence on the matter density parameter, Ω_m through style-parameters, and leveraging the Quijote Latin hypercube simulation suite (Villaescusa-Navarro et al. 2020) with 2,000 different sets of cosmological parameters as training data. The emulator delivers percentage accurate results for the nonlinear matter power spectrum in both real and redshift space at scales of $k \sim 0.6h \text{ Mpc}^{-1}$.

In this paper we demonstrate the accuracy of a 2nd-order hybrid bias expansion model that uses map2map to emulate the nonlinear displacements and velocities at the field level. This opens the door to fast, efficient, and accurate generation of many realisations across a wide range of cosmology model parameters. This has the poten-

tial to greatly improve our ability to estimate covariance matrices for summary statistics, reduce the noise in summary-statistic emulators, perform reconstruction of the dark matter distribution, and even model LSS observables at the field level.

The structure of this paper is as follows. In §2 we recap the two main tools of this study: a hybrid 2nd-order bias model (§2.1) and the map2map emulator (§2.2). Then, in §3 we present the results of our combined approach, first visually and then in terms of individual operators of the bias expansion. We then focus on two galaxy samples that mimic those in the CMASS-BOSS and EUCLID galaxy surveys. We explore the power spectrum in real and redshift space, as well as in a field-level comparison of simulated and emulated fields. We further analyse the ability of our approach to capture variations in the underlying cosmological parameters. We conclude in §4.

2 METHODOLOGY

2.1 Hybrid bias expansion model

Galaxies populate the matter field in complicated ways that have uncertain relations to environment and formation history. This connection depends on mass accretion history, mergers, and halo properties, as well as on a large variety of astrophysical processes (star formation and stellar evolution, black hole growth, feedback processes, etc). We describe this complexity by invoking a perturbative galaxy-halo connection (see e.g. Desjacques et al. 2018 for a review). The uncertainty is then handled by measuring and marginalising over the bias parameters introduced in the perturbative expansion. Specifically, at 2nd order in perturbation theory, the galaxy overdensity in Lagrangian coordinates, $\delta_g(\vec{q})$, can be written as:

$$\delta_g = 1 + b_1 \delta + b_2 (\delta^2 - \langle \delta^2 \rangle) + b_{s^2} (s^2 - \langle s^2 \rangle) + b_{\nabla} \nabla^2 \delta, \quad (1)$$

where δ is the smoothed matter overdensity in Lagrangian space (i.e. the linear overdensity field), s^2 is the traceless part of the tidal field, $s^2 = s_{ij} s^{ij} = (\partial_i \partial_j \phi - 1/3 \delta_{ij} \nabla^2 \phi)^2$, with ϕ being the linear gravitational potential, $\nabla^2 \phi = 4\pi G \bar{\rho} \delta$. The free coefficients b_1 , b_2 , b_{s^2} , and b_{∇} are referred to as Lagrangian bias parameters.

To make predictions for the tracers in Eulerian space, \vec{x} , the galaxy overdensity needs to be advected: $\delta_g(\vec{q}) \rightarrow \delta_g(\vec{x})$. This mapping can be carried out using Lagrangian perturbation theory, or, as in our hybrid approach, using N -body displacements. The hybrid approach can also be extended to redshift space, where we apply the additional velocity-dependent advection along the line-of-sight, $\delta_g(\vec{x}) \rightarrow \delta_g(\vec{s} \equiv \vec{x} + \vec{v}_z(\vec{x})/aH)$. Here v_z is the line-of-sight velocity measured in simulations.

In the BACCO implementation of hybrid biasing (Zennaro et al. 2021; Pellejero Ibañez et al. 2022; Pellejero Ibañez et al. 2023), the galaxy overdensity is written as a weighted sum of two terms modelling the contribution of central and satellite galaxies:

$$\delta_g(\vec{s}) \equiv (1 - f_s) \delta_g(\vec{s}_c) + f_s \delta_g(\vec{s}_c) *_{\vec{z}} \exp(-\lambda_{\text{FoG}} s_z), \quad (2)$$

where f_s and λ_{FoG} are two additional free parameters that represent the fraction of satellite galaxies and their typical velocity dispersion, respectively (FoG stands for Fingers-of-God, Jackson 1972; Sargent & Turner 1977). The star operation in the second term is a 1D convolution along the line-of-sight. $\vec{s}_c = \vec{x} + \vec{v}_z^c(\vec{x})/aH$ where v_z^c is the line-of-sight velocity of the parent halo. This convolution is performed on all regions of Lagrangian space that are found inside collapsed structures. The main motivation for this is that we expect

¹ https://github.com/dsjamieson/map2map_emu/

central and satellite galaxies to have very different small-scale velocities: central galaxies are predominantly at rest with respect to their halo whereas satellite galaxies have considerable random motions, giving rise to the so-called Finger-of-God effect. The magnitude of this effect scales with the virial velocity of the parent halo, but in detail depends on galaxy formation physics and the galaxy types that are sampled (see Orsi & Angulo 2018, for an extended discussion). Additionally, we consider a stochastic term $(\epsilon_1 + \epsilon_2 k^2)/\bar{n}_{\text{tr}}$ which parameterizes unmodelled small-scale physics and terms that are not included in our bias expansion (e.g. Perko et al. 2016). Here, ϵ_1 and ϵ_2 are two free parameters, and k stands for the Fourier space wavenumber.

Note that Eq. 1 is an approximation to the relationship between galaxies and dark matter, which is strictly valid only on large-scales, $\delta < 1$. As we consider smaller scales, 3^{rd} , higher-order bias terms that we have neglected can become important, potentially affecting cosmological inferences. For these reasons, the accuracy of a hybrid bias expansion needs to be monitored carefully: by checking the consistency of results with the range of scales and the order of the expansion considered and by contrasting the model against state-of-the-art galaxy formation models.

By performing the advection of Lagrangian operators with N -body displacement fields, the hybrid bias model significantly improves the accuracy of the bias expansion (Modi et al. 2020; Pellejero Ibañez et al. 2022). This is because the predictions are no longer limited by the inaccuracies of perturbation theory in predicting nonlinear displacement and velocity fields. Similarly, this approach accounts for the nonlinearity of the transformation between the Lagrangian and redshift-space coordinates (Pellejero Ibañez et al. 2022).

Previous work demonstrated that the hybrid model delivers unbiased results for the power spectrum down to scales of $k \sim 0.6 h \text{ Mpc}^{-1}$ when compared against various galaxy formation models. Specifically, Zennaro et al. (2022) showed that the hybrid model describes the galaxy auto power spectrum and its cross-correlation with matter for 8000 different catalogues spanning various cosmological models, redshifts, selection criteria, and number densities. These tests were carried out against thousands of parameter sets for SubHalo Abundance Matching extended (SHAMe, Contreras et al. 2021a,b) – an empirical extension of subhalo abundance matching that can closely resemble the hydrodynamical simulation MilkeniumTNG (Pakmor et al. 2022), as well as various semi-analytic galaxy formation catalogues. Additionally, Pellejero Ibañez et al. (2022) showed that the hybrid model can reproduce the monopole, quadrupole, and hexadecapole of the power spectrum of SHAMe galaxies in redshift space while recovering unbiased cosmological parameters (Pellejero Ibañez et al. 2023).

2.2 The map2map field-level emulator

A key ingredient of hybrid models is the displacement and velocity fields computed using N -body simulations. Unfortunately, carrying out high-resolution simulations is computationally expensive, which limits the applicability of such models. Therefore, hybrid models were previously only built for summary statistics (such as the power spectrum or kNNs, see e.g. Zennaro et al. 2021; Kokron et al. 2021; Yuan et al. 2023). While these will be valuable tools for analysing upcoming LSS observations, they fall short of fully exploiting the method and the data.

The emergence of field-level emulators offers an ideal companion to hybrid biasing. These emulators provide computationally efficient methods to generate displacement fields with accuracy comparable to N -body simulations over the range of scales where hybrid bi-

asing is applicable. In this work we employ the latest incarnation of map2map field emulator, presented by Jamieson et al. (2022). map2map employs convolutional neural networks (CNNs) to predict the nonlinear displacement and velocity fields of a given region of the Universe. These CNNs receive the 1st-order LPT displacement field together with the value of the matter density parameter Ω_m as inputs.

Specifically, map2map uses two CNNs with a 4-tier V-Net architecture. The loss function for the displacement V-Net was set as a linear combination of the logarithm of the mean squared error (log-MSE) in the Lagrangian displacements of particles and the Eulerian density field. For the velocity V-Net, the loss function was set as the sum of the log-MSE in the particle velocities, the Eulerian momentum field, and the second moment of the Eulerian momentum field.

The emulator was trained using ~ 1700 N -body simulations of the Quijote suite (Villaescusa-Navarro et al. 2020), which have distinct cosmological parameters sampled on a Latin hypercube over the 5-dimensional parameter space:

$$\Omega_m \in [0.1, 0.5], \quad (3)$$

$$\Omega_b \in [0.03, 0.07], \quad (4)$$

$$h \in [0.5, 0.9], \quad (5)$$

$$n_s \in [0.8, 1.2], \quad (6)$$

$$\sigma_8 \in [0.6, 1.0]. \quad (7)$$

Each of these simulations evolved 512^3 particles over a $1 h^{-3} \text{ Gpc}^3$ volume, which corresponds to a particle mass resolution range $m_p \approx 2 \times 10^{11} - 1 \times 10^{12} M_\odot h^{-1}$.

2.3 The emulated galaxy bias field

To validate our approach, we build two biased fields that resemble galaxy samples typically targeted by LSS observational surveys.

- **LRGs:** The first set mimics massive galaxies, such as those targeted by the BOSS-CMASS samples. Specifically, we employ a set of Lagrangian bias parameters $\{b_1, b_2, b_{s^2}, b_\nabla, \lambda_{\text{FoG}}, f_{\text{sat}}\} = \{0.45, 0.15, 0.52, -1.8, 0.4, 0.2\}$, and a number density of $\bar{n} = 4 \times 10^{-4} / D^2(z = 0.61) = 2.3 \times 10^{-4} [\text{Mpc}/h]^{-3}$. We refer to this sample as Luminous Red Galaxies, LRGs.

- **ELGs:** The second set aims to resemble emission line galaxies such as those to be targeted by the DESI and EUCLID surveys. We employ $\{b_1, b_2, b_{s^2}, b_\nabla, \lambda_{\text{FoG}}, f_{\text{sat}}\} = \{0.38, -0.36, 1.44, -1.35, 0.4, 0.2\}$ with a density of $\bar{n} = 6 \times 10^{-4} / D^2(z = 1) = 2.2 \times 10^{-4} [\text{Mpc}/h]^{-3}$. We refer to this sample as Emission Line Galaxies, ELGs.

Note that the value of the bias parameters was set so that the resulting galaxy power spectrum closely matches that of physically-motivated galaxy formation models. Specifically, for the LRG's we choose the values provided by Pellejero Ibañez et al. (2022) that best fit the clustering of stellar-mass selected galaxies as predicted by the SHAMe model with parameters that reproduce results in the TNG300 hydrodynamical simulation. For the ELG sample, we used the best-fit parameters of the Euclid mocks Model 3, as explained in Pozzetti et al. (2016). In addition, since the map2map emulator has only been trained at $z = 0$, we use this redshift for our analysis but tune the value of the discreteness noise so that the ratio $P(k = 0.2)/\bar{n}$ is the same between our $z = 0$ catalogue and that expected for LRG and ELG samples at $z = 0.61$ and $z = 1$, respectively. When computing the 2-point statistics of the simulated galaxy bias fields, we further set the stochastic parameters $\{\epsilon_1, \epsilon_2\}$ to zero.

Operationally, we start by defining a specific realisation of the initial Gaussian field on a $V = 1h^{-3}\text{Gpc}^3$ using 1024^3 grid points, which we then smooth on a scale $k_d = 0.75h\text{Mpc}^{-1}$. We then build all 5 operators, $\{1, \delta, \delta^2, s^2, \nabla^2\delta\}$, advect them to Eulerian space and subsequently to redshift space if appropriate. We do this either using displacement fields from `map2map` or from one of the Quijote N -body simulations. These advected fields are finally combined and weighted with the appropriate bias parameters to retrieve a galaxy-like biased field.

We will quantify the accuracy of the emulator combined with the hybrid bias expansion by comparing statistics of the fields generated with `map2map` to those constructed from the original Quijote simulations. Although `map2map` has previously been shown to deliver accurate predictions for the nonlinear power spectrum, achieving similar performance for the biased field is not guaranteed. The bias operators weigh various parts of the cosmic web differently. This could potentially reveal shortcomings of the emulated fields that do not significantly contribute to the unbiased, dark matter power spectrum.

2.3.1 Test suite

We employ two different datasets to evaluate the accuracy of our approach. The first one corresponds to 100 randomly-selected realisations of the “fiducial”-cosmology simulations of the Quijote suite: $\Omega_m = 0.3175$, $\Omega_b = 0.049$, $\sigma_8 = 0.834$, $h = 0.6711$, and $n_s = 0.96$. These simulations have the same volume and spatial resolution employed for the training of the `map2map` emulator. With this suite, we characterise the typical accuracy of `map2map` in predicting galaxy statistics. The second test suite corresponds to another 100 simulations with varied cosmological parameters. These were not employed during training, which allows us to quantify the ability of `map2map` at capturing the correct cosmology dependence.

2.3.2 Computational performance

In addition to the robustness against galaxy formation physics, a key advantage of our approach is its computational efficiency. Unlike other approaches, such as halo occupation distribution, we do not rely on halo group finding or high spatial resolution, which makes our approach extremely computationally efficient.

To generate a $V = 1h^{-3}\text{Gpc}^3$ galaxy field, our model requires approximately 2.5 minutes of CPU time. Of this, approximately 30 seconds is employed to generate an initial density field and the bias operators; 15 seconds for computing 1LPT displacements, and 1 minute for augmenting them with `map2map`. A final 15 seconds is required for the advection and calculation of the full Eulerian field. In redshift space, an extra minute is required for the computation of the non-linear velocity components by `map2map`, although this could be further parallelized by running the velocity model on a separate node.

3 RESULTS

3.1 Visual inspection

We first illustrate the performance of our approach in Fig. 1 which compares the predictions for the ELG-like galaxy sample at the fiducial cosmology using either N -body or emulated displacements fields. As we have argued above, the hybrid bias is expected to perform well on scales $k < 0.6h\text{Mpc}^{-1}$ (at least at the 2-point statistics

level). Therefore, we display fields after smoothing with a Gaussian filter of size $\pi/0.6 \approx 5h^{-1}\text{Mpc}$.

By comparing the top two left panels, we can appreciate a striking similarity between the emulated and simulated biased density fields. In particular, the location of voids, filaments, and overdensities coincides almost perfectly. We see that our approach is indeed capturing the non-Gaussian features of the galaxy density field. In the bottom two panels, we provide the ratio between these two predictions, we see that if displacements are provided by 1LPT (i.e. the Zeldovich Approximation, ZA), then there exist larger residuals that have a coherence length of up to hundreds of Mpc. The typical value of the residuals decreases by several orders of magnitude when `map2map` displacements are used instead.

As shown by the right-side regions of Fig. 1, the accuracy of our approach is also high for the velocity field. Whereas the ZA residuals display values of up to 50% that are coherent over tens of Mpc, the `map2map` emulation greatly decreases these errors. We do find residual differences at the borders of halo structures. This indicates a possible limitation in our approach and an avenue for potential improvement: extending the emulator’s ability to predict the interior of collapsed regions in N -body simulations. However, as we will demonstrate below, it is possible to absorb some of these residual differences by incorporating them into the nuisance parameters of the model, which minimises their impact on our predictions. We explore further the performance of our model next.

3.2 2nd-order operators

As explained earlier, any galaxy field is described by a sum of 5 fields weighted by their respective bias parameters under the 2nd-order hybrid bias expansion. This implies that any galaxy power spectrum will be described as a linear combination of 15 cross-power spectra.

We show these power spectra in Fig. 2 at $z = 0$ for the fiducial cosmology of the Quijote suite. Each panel shows a distinct set of spectra. The symbols correspond to results obtained from fields advected using the the N -body simulation displacements averaged over 100 realizations, with error bars depicting the standard deviation among these. Solid lines show the corresponding measurement but using `map2map` emulated displacements. For comparison, the spectra computed using 1LPT displacements are shown as dotted lines.

Overall, we see excellent agreement for all 15 spectra over the full range of scales considered. The `map2map` emulator is able to correct for the non-linearities missing in the 1LPT approach. Specifically, the P_{11} , $P_{1\delta}$, and $P_{\delta\delta}$ terms – which dominate on large scales – are all almost indistinguishable between the simulation and emulation results. On smaller scales, quadratic terms ($P_{\delta^2\delta^2}$ and $P_{\delta\delta^2}$) become increasingly important. These are also extremely well reproduced.

We can better appreciate the accuracy of `map2map` in Fig. 3, which shows the fractional difference among each of these cross spectra. For clarity, we have displayed the differences relative to the standard deviation measured among the Quijote realisations. As in the previous figure, the dotted lines depict results from 1LPT. The error bars correspond to the $1-\sigma$ scatter measured among the `map2map` spectra. Therefore, the closer this scatter is to 1, the better the diagonal terms of the covariance matrix are recovered. We will explore this further in a subsequent section.

On large scales, $k < 0.1h\text{Mpc}^{-1}$, the emulated and simulated cross-spectra are in good agreement. The 1LPT predictions, on the other hand, deviate from our simulation results on scales $k \sim 0.05h^{-1}\text{Mpc}$. On smaller scales, we detect systematic deviations – depending on the spectra, `map2map` can overpredict or underpredict the signal by up to 3σ . Note that the magnitude of this bias is nev-

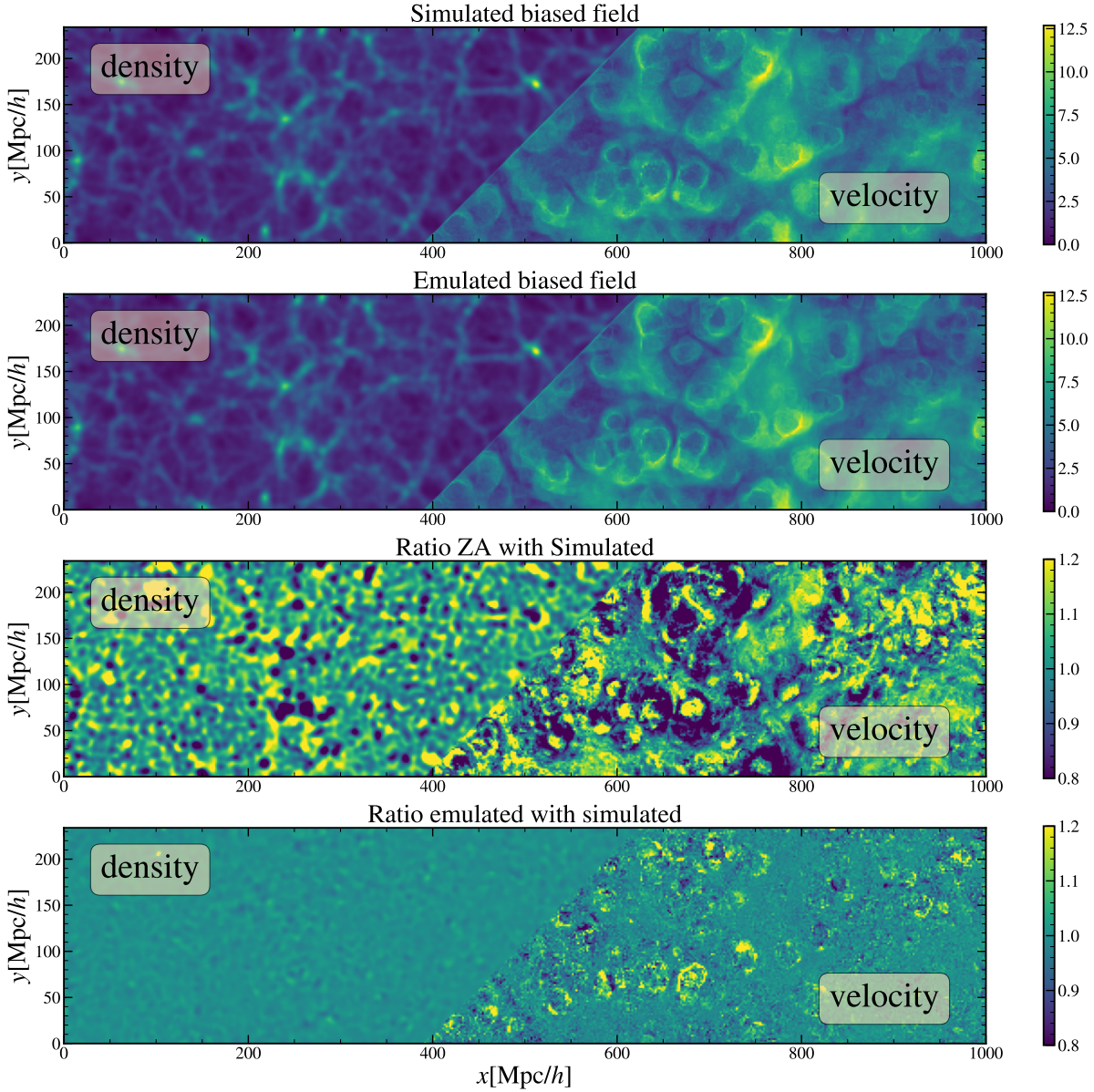


Figure 1. Comparison between biased fields computed using N -body simulations and the `map2map` emulator. The figure shows a case study that emulates an ELG galaxy sample at $z = 0$ over a spatial region of $1000h^{-1}\text{Mpc} \times 250h^{-1}\text{Mpc}$ with a depth of $15h^{-1}\text{Mpc}$. The left and right regions of each panel depict the projected matter density and the modulus of the peculiar velocity $||\vec{v}||$, respectively. The velocity field is constructed by incorporating the velocities of the halos and the velocities of the dark matter particles not associated with any halo, as required by the hybrid model. The top panel displays the results obtained from simulated displacement and velocity fields, while the second panel showcases the corresponding outcomes using emulated quantities. For comparison, the third panel presents the ratio with respect to 1LPT. The lower panel shows the ratio between the simulated and emulated results.

ertheless extremely small. For the P_{11} term this error corresponds to a bias of 1.5% at $k = 1h\text{Mpc}^{-1}$. We present the corresponding redshift space results in Appendix A. The redshift space results include the central velocity (v_z^c) distortion effect, which differs between `map2map` and Quijote. This leads to enhanced errors compared to the real space operators. The absolute and relative importance of the uncertainty in each $P_{i,j}$ does, however, depend on the specific set of bias parameters describing a given galaxy sample, which is what we investigate next.

3.3 Power spectrum

In this subsection, we compare the power spectrum of biased tracers obtained from emulated and simulated displacement fields. By using two different methods to fit the four nuisance parameters $\epsilon_1, \epsilon_2, f_{\text{sat}}, \lambda_{\text{FoG}}$ in the model, we obtain two distinct sets of results. The first set (named *emulated*) is comprised of outcomes where the nuisance parameters are fixed from the N -body data, and prevented from absorbing any errors arising from the emulated displacements. The second set (named *calibrated*) incorporates the ability of the nuisance parameters to accommodate any inaccuracies in the emula-

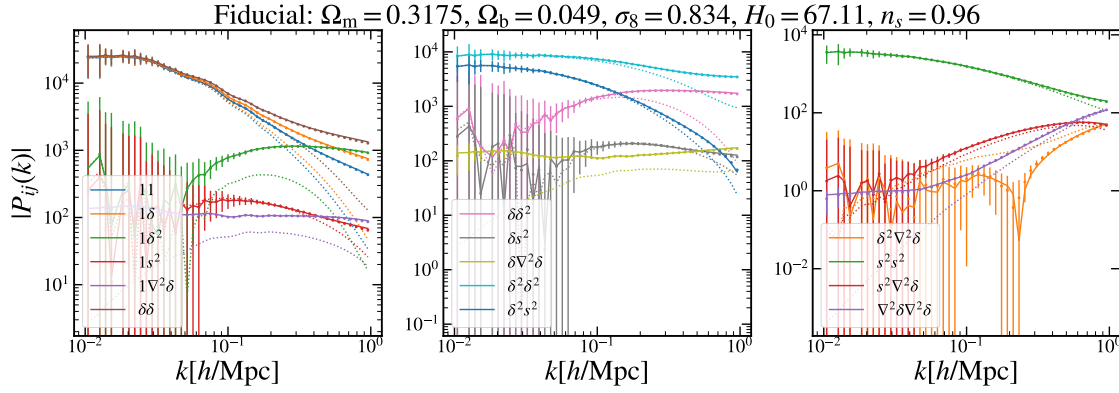


Figure 2. Power spectra of the 15 different operator fields at $z = 0$ that determine a 2nd-order bias expansion, as indicated by the legend. We display our results at the fiducial cosmology of the Quijote suite, the parameter values are displayed in the figure title. For each of the power spectra, symbols display the average over 100 N -body realisations of a $1h^{-3}\text{Gpc}^3$ volume, whereas solid lines display the same quantity as predicted by map2map. Vertical error bars indicate the standard deviation of the N -body ensemble. The dotted lines represent the 1LPT predictions that map2map takes as input.

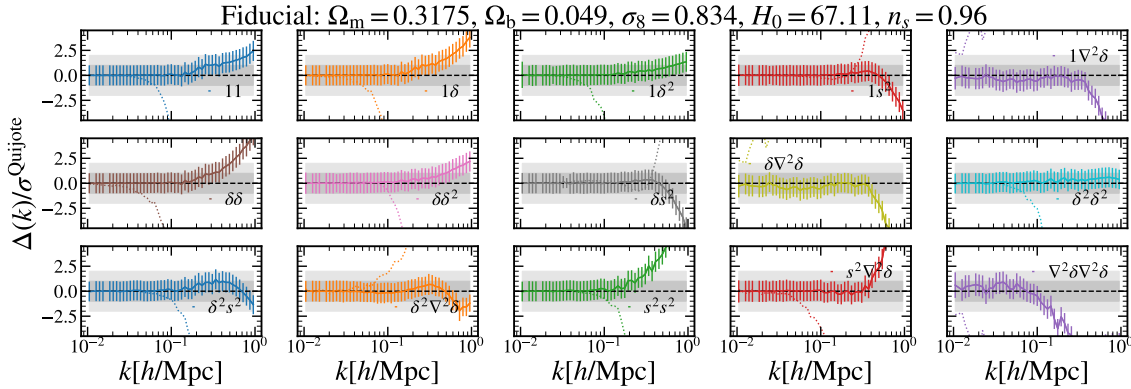


Figure 3. Relative difference between the predictions of map2map and measurements in the Quijote suite, in units of the simulation variance for a $1h^{-3}\text{Gpc}^3$ volume, $(P_{\text{m2m}} - P_{\text{Quijote}})/\sigma_{\text{Quijote}}^2$. Each panel shows results for a different pair of operator fields advected to $z = 0$, as indicated by the labels on each panel. We display the average and standard deviation over 100 realisations as solid lines and vertical error bars, respectively. For comparison, dotted lines show the predictions from 1LPT displacements.

tor. Note that both *emulated* and *calibrated* results are obtained from the map2map emulated displacements.

3.3.1 Real space

We compare the real-space power spectra of biased fields in the leftmost column of Fig. 4. LRG and ELG tracers are displayed by red and blue lines, respectively. In the top panel, we show the mean of our 100 test realisations. The expected scale of validity of the hybrid approach, $k \sim 0.6h^{-1}\text{Mpc}$, is marked by a vertical dot-dashed line in the lowest panel.

The map2map results are almost indistinguishable from those obtained from the simulations, which quantitatively confirms our previous findings. As we show in the bottom panels of Fig. 4, the fractional differences are subpercent on all scales for ELGs and barely 1% at $k \sim 1h^{-1}\text{Mpc}$ for the LRG sample. These differences, however, are statistically significant given the volume of our simulations ($V = 1h^{-3}\text{Gpc}^3$), reaching 2σ at $k \sim 0.6h^{-1}\text{Mpc}$. Despite this, we show that these small differences can be absorbed by the free param-

eters of the hybrid bias model. Specifically, in the bottom panel we adjust the value of the free parameters ϵ_1 and ϵ_2 , which are typically interpreted as describing stochastic noise and truncated terms in the hybrid bias model. The differences are now almost absent, meaning the errors introduced by the emulator are predominantly degenerate with the errors associated with the approximations of the hybrid model itself. After freely varying the nuisance parameters, the excess error associated with the emulator is negligible.

3.3.2 Redshift space

A more challenging test is to reproduce the multipoles of the redshift-space power spectrum. The emulator not only needs to correctly displace Lagrangian elements to Eulerian space, it also needs to assign their correct nonlinear velocity. For our model, this task also requires knowing whether a particle is part of a halo or not.

We show our results in the right panels of Fig. 4. Second, third, and fourth panels show the results for the monopole ($\ell = 0$), quadrupole ($\ell = 2$), and hexadecapole ($\ell = 4$), of the power spectrum. As in

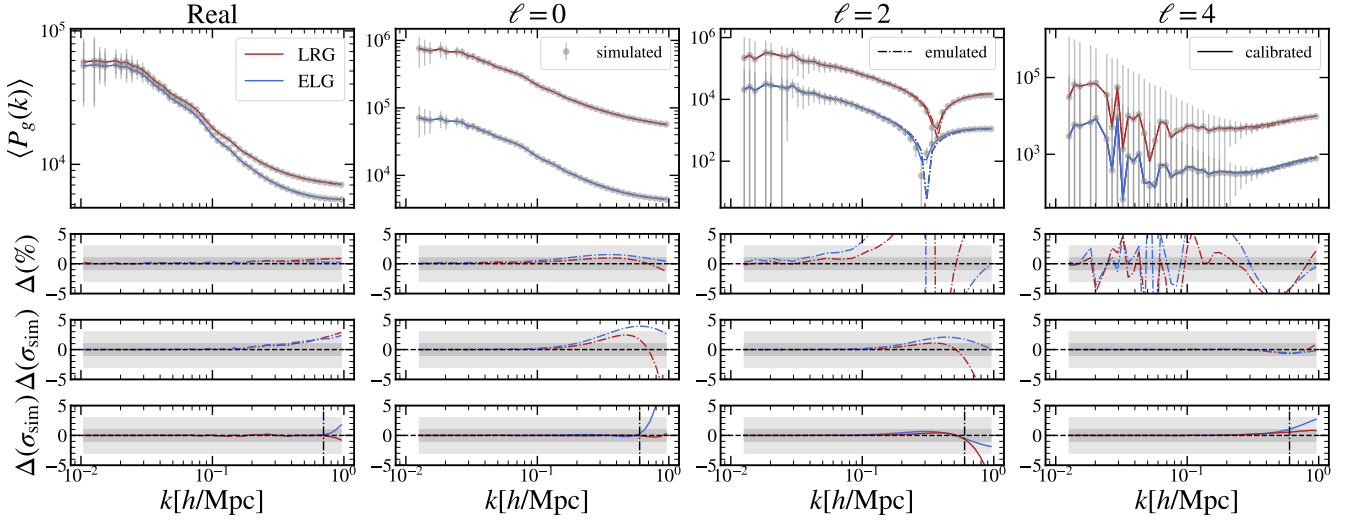


Figure 4. Comparison between the power spectra of LRG and ELG biased fields employing either Quijote simulations or the map2map field emulator. LRG results have been displaced by one order of magnitude to clearly distinguish them. We show the results for the mean of 100 realisations in a $1h^{-3}\text{Gpc}^3$ volume. Bottom panels display the relative differences in various manners: first showing the percentage difference and then in units of the variance measured in the Quijote suite. In the bottom panel, we also show the case where the noise and FoG parameters in emulated galaxy fields have been calibrated to match the simulated results.

previous figures, LRG and ELG galaxies are shown with red and blue lines, respectively. For clarity, we have vertically displaced the LRG results by one order of magnitude. Bottom panels show both the percentage relative differences and the differences relative to the variance as measured in our test suite.

We see that the monopole is recovered better than 2% for both galaxy samples. The errors from both emulated galaxy samples, however, display a bump on small scales, which can be of around 5σ in magnitude at $k = 0.6h^{-1}\text{Mpc}$. The quadrupole shows a consistent picture: large scales are accurately recovered by map2map but small scales are enhanced and then washed out relative to the simulated galaxy fields. The associated errors can be up to 3σ at $k \sim 0.6h^{-1}\text{Mpc}$. The hexadecapole is less sensitive to these inaccuracies and map2map is statistically unbiased over almost all the range of scales we explored.

The origin of these discrepancies is an additional small-scale velocity dispersion in the map2map predictions. In the BACCO hybrid model, Lagrangian elements that are inside haloes are assigned exactly the same velocity, given by the center of mass velocity of the parent halo. This is a challenging quantity to predict for map2map, since it needs to correctly predict which Lagrangian elements will become part of a halo based on the displacement field. It also needs to accurately detect the boundaries of halos to distinguish the transition between particles outside and inside halos. Although not shown here, we have verified that map2map does display an additional velocity dispersion in and around haloes. While the magnitude of this velocity is small, it is statistically significant.

There are two possible alternatives to address this issue. The first one is to improve the accuracy of map2map. This can be achieved by either increasing the training data, improving the network architecture, or exploring an alternative formulation of the redshift-space hybrid model in terms of quantities that map2map can predict more easily. The second alternative is to redefine the meaning of the nuisance parameters of the hybrid model so that they account for the additional velocity dispersion in map2map. Specifically, our RSD

model contains a parameter λ_{FoG} that controls the amount of velocity dispersion our modelled galaxies display inside halos. The actual value of this parameter depends on the galaxy selection. Even for a sample of purely central galaxies, we expect a small-scale velocity dispersion arising from the relative velocity between these galaxies and their host halos (an effect commonly referred to as velocity bias). Therefore, we expect λ_{FoG} to be degenerated with the intrinsic scatter of the emulation.

In the bottom-most panel of Fig. 4 we compare our simulated galaxies with map2map after fitting the values of our noise and RSD nuisance parameters $\{\epsilon_1, \epsilon_2, f_{\text{sat}}, \lambda_{\text{FoG}}\}$. As we had anticipated, we see that the freedom in our model is sufficient to absorb the effect of map2map inaccuracies, delivering power spectrum multipoles that are almost indistinguishable from the simulated results. When considering the monopole, the primary dependencies are absorbed by the parameters ϵ_1 and ϵ_2 . In contrast, for the quadrupole and hexadecapole, these dependencies are absorbed by the parameters f_{sat} and λ_{FoG} , which effectively account for the influence of map2map intrinsic scatter.

To place our results in context, we consider the case of the Euclid survey. Euclid is expected to observe 15,000 sq deg in bins of $\Delta z \sim 0.2$, which corresponds to approximately $10h^{-3}\text{Gpc}^3$ – 10 times the volume of each Quijote simulation. Even for this case, where the precision of the measurement would be approximately 3 times better than in our tests, we expect the accuracy of map2map to affect the analysis only at scales where $k \gtrsim 0.3h\text{Mpc}^{-1}$. Note that we could also calibrate our free parameters for lower k -values than $k \sim 0.6h\text{Mpc}^{-1}$ to alleviate the emulator errors here.

3.3.3 Variance

Combining the hybrid bias model with map2map emulation significantly enhances the speed and efficiency of mock generation, enabling the estimation of large covariance matrices. Accurate covariance estimation is typically limited by the cost of generating the

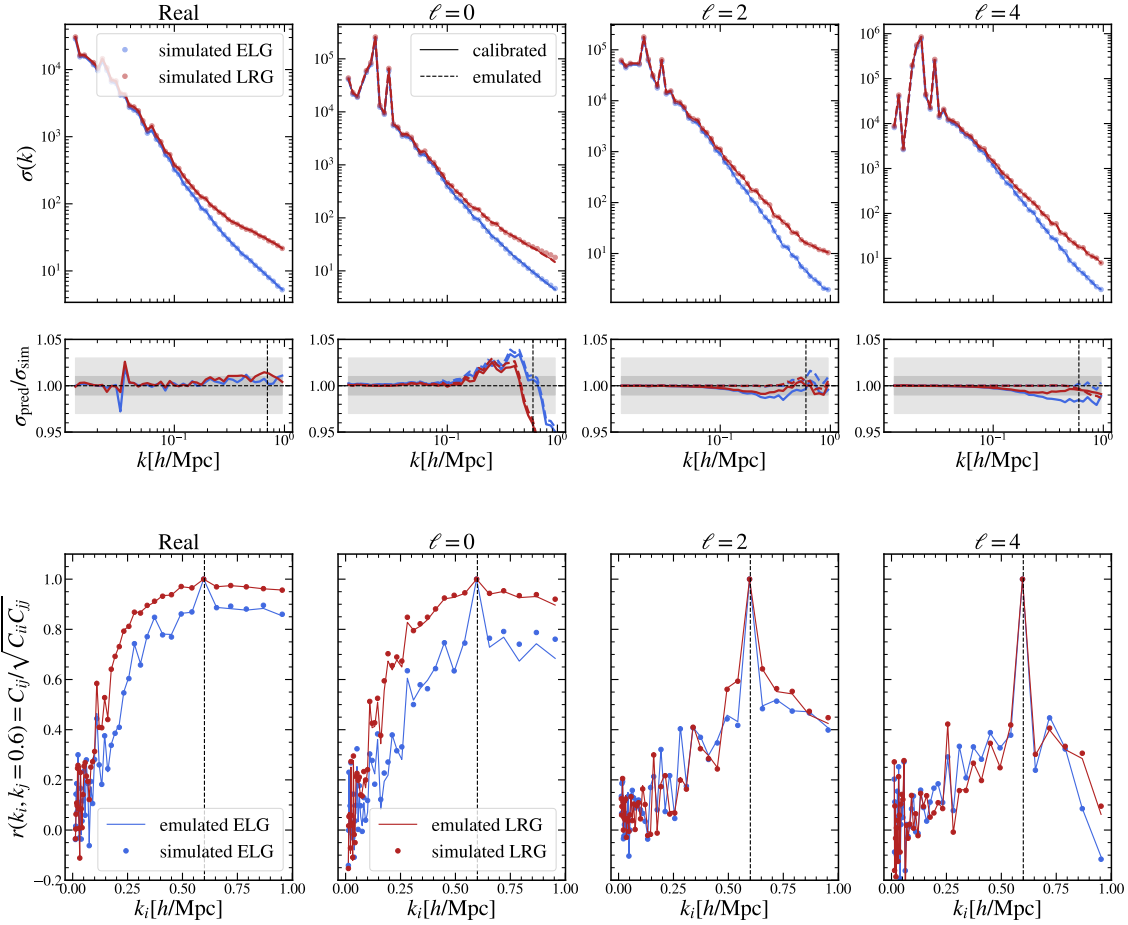


Figure 5. Upper Panels: the standard deviation predicted by `map2map` before and after marginalization over the noise and FoG (Finger-of-God) nuisance parameters. The scatter, represented by points, corresponds to the Quijote standard deviation. Crosses indicate the Quijote standard deviation after applying FoG. The thick lines display the scatter recovered from `map2map` results, while the dashed lines indicate the `map2map` results after marginalization over the nuisance parameters. The different lines indicate the accuracy for distinct galaxy samples, namely LRG (Luminous Red Galaxies) and ELG (Emission Line Galaxies). Lower Panels: the elements of the correlation coefficients matrix at a fixed $k_j = 0.6 h \text{ Mpc}^{-1}$. These results are shown exclusively after marginalization over the nuisance parameters. The dashed line denotes $k_j = 0.6 h \text{ Mpc}^{-1}$, which corresponds to the point of maximum correlation.

enormous number of realisations needed to reduce both the noise and the bias of our estimators (see e.g. [Dodelson & Schneider 2013](#)). This is crucial for obtaining rigorous constraints from large-scale structure observations. Our combined approach offers an ideal solution by enabling the creation of millions of accurate realizations at a moderate computational cost.

To validate our approach, we perform a comparison between the diagonal elements of the covariance matrix obtained from our suite of 100 simulations and those obtained from the corresponding emulated galaxy fields. The upper panels of Fig. 5 depict these comparisons for both ELG and LRG samples, considering real space and the multipoles of the redshift-space power spectra. We present results for both the emulated model and the calibrated model, in which the nuisance parameters of the bias model have been refitted to accurately describe the emulated galaxy power spectra. It is worth noting that the parameters ϵ_1 and ϵ_2 have no impact on the covariance since they simply contribute constant values to the mean. Conversely, the redshift space nuisance parameters do influence the covariance as they enter through convolutions of the fields.

We find that `map2map` is indeed able to accurately recover the variance of the power spectra. The deviations from the N -body values are smaller than 3% and typically at subpercent levels. To put these numbers in context, [Blot et al. \(2019\)](#) performed a covariance matrix challenge based on the Minerva simulation suite ([Grieb et al. 2016a](#)), where the typical accuracy reached 5-10% down to scales of $k \sim 0.2 h \text{ Mpc}^{-1}$. More recent work, such as those of the BAM team have reached subpercent results using similar ideas to machine learning approaches (see [Balaguera-Antolínez et al. 2019a; Balaguera-Antolínez et al. 2019b; Pellejero-Ibañez et al. 2020; Sinigaglia et al. 2021; Kitaura et al. 2022](#), and [Balaguera-Antolínez et al. 2023](#)).

Our findings reveal that the calibration process yields a slight enhancement in the monopole signal-to-noise ratio. However, it also leads to an apparent degradation in the variances of the quadrupole and hexadecapole spectra on intermediate scales. Although not shown here, the value of σ/P seems, however, unaffected. Nevertheless, even with this degradation, the values remain within a 2% range of accuracy.

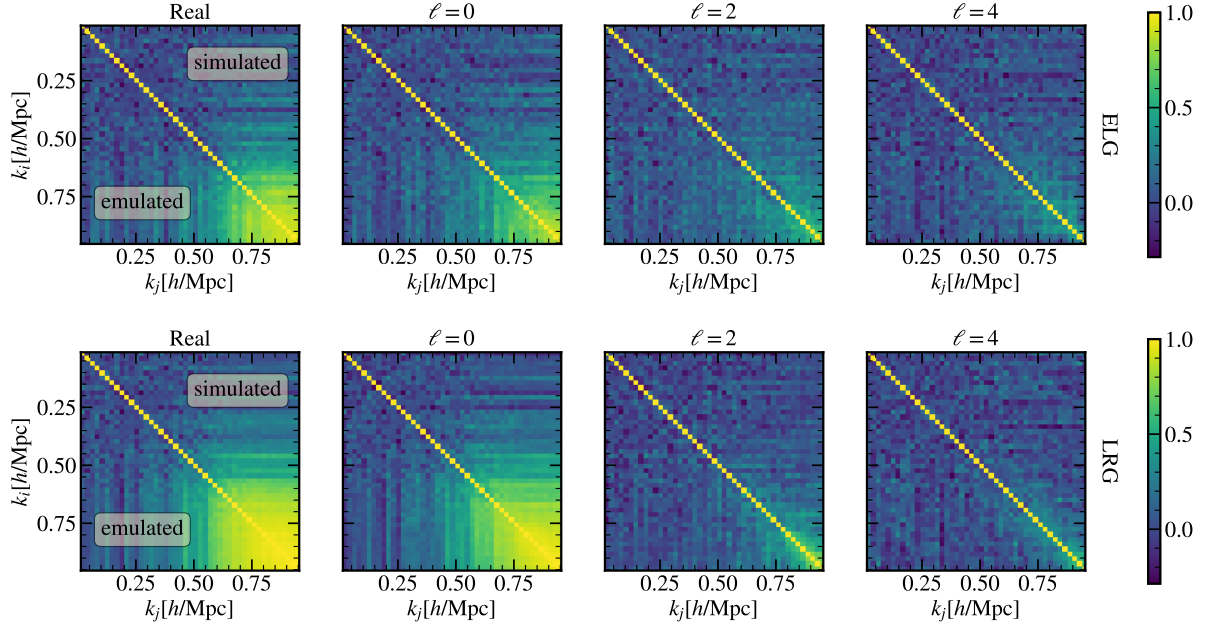


Figure 6. Correlation matrices for the ELG and LRG samples. The correlation coefficient, defined as $r(k_i, k_j) = C_{ij} / \sqrt{C_{ii}C_{jj}}$, is used to measure the correlation between different wavenumbers k_i and k_j . The lower triangles of the matrices illustrate the results obtained from the `map2map` emulator, while the upper triangles display the corresponding outcomes from the Quijote simulations conducted under the fiducial cosmology.

In the lower panels of Fig. 5, we present the correlation coefficients $r(k_i, k_j)$ at $k_j = 0.6h \text{ Mpc}^{-1}$ for both real and redshift space outcomes. These coefficients are defined as $r(k_i, k_j) = C_{ij} / \sqrt{C_{ii}C_{jj}}$, where C_{ij} represents the covariance matrix obtained from 100 independent samples under the fiducial cosmology. Our analysis reveals no significant deviations, indicating that the `map2map` emulator successfully captures the nondiagonal terms of the covariance. The complete structure of the correlation coefficients is illustrated in Fig. 6. The lower triangular sections of the matrices display the emulated results, whereas the upper triangular regions depict the simulated results. Upon visual inspection, the structures appear indistinguishable, suggesting that `map2map` accurately reproduces the four-point functions as predicted by the hybrid bias model.

There remain several aspects that require further validation before using the approach introduced here for covariance estimation. For instance, the ability of the hybrid bias model to correctly reproduce the expected covariance (i.e. testing whether the trispectrum is well described, the role of higher-order bias parameters, etc), and extensions of `map2map` to lightcones and higher redshifts need to be further developed and explored. We plan to carry out these investigations in future work.

3.3.4 Field-level

In previous sections we explored results for 2-point statistics, which facilitate interpretation and analyses that are familiar and easy to understand. The advantage of our model is that it provides predictions for the complete three-dimensional field, as illustrated in Fig. 1, which allows us to go beyond 2-point statistics and consider the field-level information content. This has the potential to significantly increase the constraining power of extra-galactic survey observations (e.g. Porqueres et al. 2023). Therefore, we now shift our focus to assessing the accuracy of `map2map` at the field level.

The accuracy of field-level information can be assessed using various methods (see e.g. Cabass & Schmidt 2020; Villaescusa-Navarro et al. 2021). Here, we adopt the approach presented in Schmittfull et al. (2019), which computes the power spectrum of the difference between the simulated and emulated overdensity fields: $\Delta(k) \equiv \langle |\delta_g^{\text{sim}} - \delta_g^{\text{m2m}}|^2 \rangle$. Essentially, this corresponds to measuring the expected difference in the amplitude of each Fourier mode as predicted by the simulation and the emulation. As with the case of the 2-point statistics, we will examine and compare two scenarios: one where we consider only deterministic contributions to the galaxy field, disregarding the stochastic parameters ϵ_1 and ϵ_2 , and another where we incorporate the contributions from these stochastic parameters. We compare these results against the expected Gaussian variance of each Fourier mode, $\sigma(k) = \sqrt{2/N_{\text{modes}}(P(k) + 1/\bar{n})}$. Since on small scales we expect additional non-Gaussian contributions to the variance, our results will provide a conservative estimate to the accuracy of our hybrid approach.

We show the results of computing the mean of $\Delta(k)$ over the 100 fiducial cosmology simulations as red and blue lines in Figure 7. The dash-dotted lines represent the results of the emulation. The figure indicates that real fields (upper panel) are recovered by `map2map` with an error smaller than the expected contribution of discreteness noise down to scales of $\sim 0.6h \text{ Mpc}^{-1}$ (similar to the results found for the power spectrum). Thick lines show results after the absorption of emulator errors by the nuisance parameters of the model, which yields unbiased results down to scales of $\sim 1h \text{ Mpc}^{-1}$.

In the second, third, and fourth panels of Figure 7, we present redshift space results. The values of $\sigma(k)$ represent the scatter within each k -bin, as estimated using the Gaussian approximation described in Grieb et al. (2016b). The emulated results start to deviate at scales of approximately $\sim 0.3h \text{ Mpc}^{-1}$ for the monopole, $\sim 0.35h \text{ Mpc}^{-1}$ for the quadrupole, and $\sim 0.6h \text{ Mpc}^{-1}$ for the hexadecapole. Calibrating nuisance parameters leads to improvement

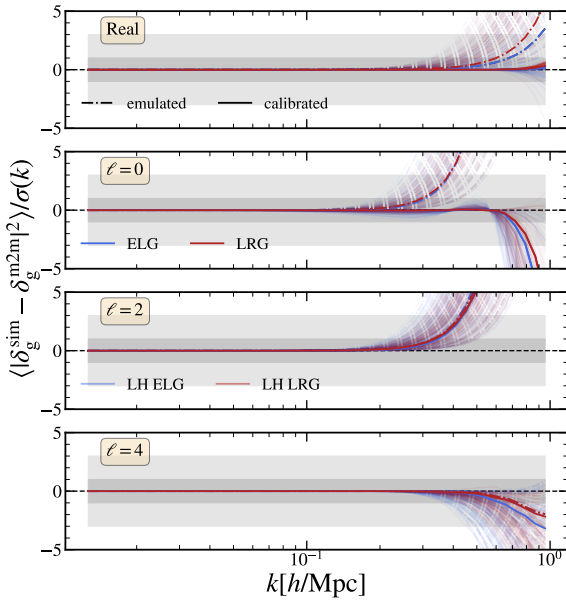


Figure 7. Expected difference in the amplitude of each Fourier mode between the LRG and ELG galaxy simulated fields as predicted by `map2map` compared to the Quijote simulations weighted by the Gaussian variance at each Fourier mode. The presented panels include results for real space and redshift space multipoles of the field residuals. The thick coloured lines indicate the average results obtained from 100 Quijote simulations at the fiducial cosmology. The semi-transparent lines represent individual results from 100 Quijote simulations randomly selected from the Latin Hypercube (LH) space cosmologies. Dash-dotted lines indicate results from the emulation of the fields directly. Full lines represent results after calibration through the free nuisance parameters.

in the monopole, achieving accuracy within 1σ down to scales of around $\sim 0.7h \text{ Mpc}^{-1}$. On the other hand, the quadrupole and hexadecapole are largely unaffected by the calibration. Note that the quadrupole and hexadecapole are mainly affected by the FoG parameters and are independent of the noise parameters. Therefore, it is possible that higher-order terms in the noise expansion may absorb the residual dependencies observed in this figure. We plan to explore these terms, which typically have $k^2\mu^2$ dependencies (Perko et al. 2016), in future studies.

Our results indicate that `map2map` can serve as a valuable tool for cosmological parameter inference at the field level. However, robust field-level parameter inference using the proposed hybrid model in combination with `map2map` still requires two further validation tests. First, we must demonstrate that the results obtained from `map2map` emulation hold when cosmological parameters are varied. Second, we need to investigate whether the hybrid model can deliver unbiased cosmological constraints at the field level. We focus on the first one next and leave the second for future work.

3.4 Cosmology dependence of the `map2map` emulator

As mentioned earlier, our combined approach shows great promise for analyzing LSS and placing constraints on cosmological parameters. A key advantage of our approach lies in its flexibility over the

choice of which statistics to analyze, since it predicts 3-dimensional galaxy fields. The effectiveness of incorporating `map2map` into these analysis strategies depends on it reliably predicting the cosmological dependence of the 5 advected Lagrangian fields in our bias expansion.

We explore this issue in Fig. 8, where we compare the `map2map` predictions for ELG and LRG galaxy power spectra in 100 different cosmologies of the Quijote Latin Hypercube suite. Specifically, we display the difference in units of the fiducial standard deviation between these two estimates at the wavenumber $k = 0.6h \text{ Mpc}^{-1}$ as a function of the value of Ω_m , Ω_b , h , n_s , and σ_8 . Note we employ the calibrated versions of our parameters where the noise and RSD nuisance parameters are chosen so that they capture inaccuracies in `map2map`. These parameters are varied to fit each cosmology independently, as it would be done in an analysis of observational data.

The accuracy we achieve when varying cosmological parameters is almost entirely consistent with the results found earlier at the fixed, fiducial cosmology. The errors are within $1\sigma_{\text{sim}}$ for the real and redshift space power spectra. The only exception is the hexadecapole, where the emulator’s inherent scatter results in values exceeding $1\sigma_{\text{sim}}$, particularly for the ELG sample. We have checked that this agreement extends to the range of scales shown in the bottom-most panel of Fig. 4. This is a remarkable result as it demonstrates that `map2map` is capable of generating biased fields at the level of scatter observed in N -body simulations across a broad range of cosmologies and scales.

We find the only significant cosmology dependence of the errors is on σ_8 , which exhibits marginal trends that are consistent across different statistics. Specifically, for lower values of σ_8 , we observe lower deviations and reduced scatter. Conversely, for typical values of $\sigma_8 > 0.8$, the scatter doubles, and the deviations become more pronounced. The most prominent example is the hexadecapole, which exhibits deviations of up to $2\sigma_{\text{sim}}$ for $\sigma_8 \sim 0.95$. This trend aligns with the findings of Jamieson et al. (2022), although in their case, the lack of a calibration procedure exacerbates these effects. Fixing this dependency goes beyond the scope of this paper and we leave it for further work.

The cosmology dependence of field-level results are shown in Fig. 7. The semi-transparent lines represent the root mean square (r.m.s) of each Fourier mode weighted by their expected scatter, serving as a measure of the field-level recovery when changing cosmological parameters. Our findings demonstrate that the results obtained with `map2map` remain roughly consistent with those obtained in the fiducial cosmology at the field level. Some cosmologies in redshift space show differences of $\pm 0.05h \text{ Mpc}^{-1}$ in accuracy with respect to the fiducial cosmology, but most lie within less than $\pm 0.02h \text{ Mpc}^{-1}$. Remarkably, both real and redshift spaces are accurately reconstructed by `map2map`, surpassing the expected noise levels for present surveys down to scales of $\sim 0.35h \text{ Mpc}^{-1}$. These consistent and reliable predictions across various cosmologies indicate the robustness and versatility of `map2map`, opening up opportunities for diverse applications in field-level analysis.

4 CONCLUSIONS

In this paper, we have explored the idea of combining a field-level emulator with a hybrid bias expansion. Our emulator, `map2map`, takes the 1LPT prediction as input and transforms it with a CNN model to predict the expected nonlinear displacement and velocity fields at $z = 0$. In turn, the hybrid bias expansion is a general way to describe the abundance of galaxies. Combining the emulated nonlinear advection

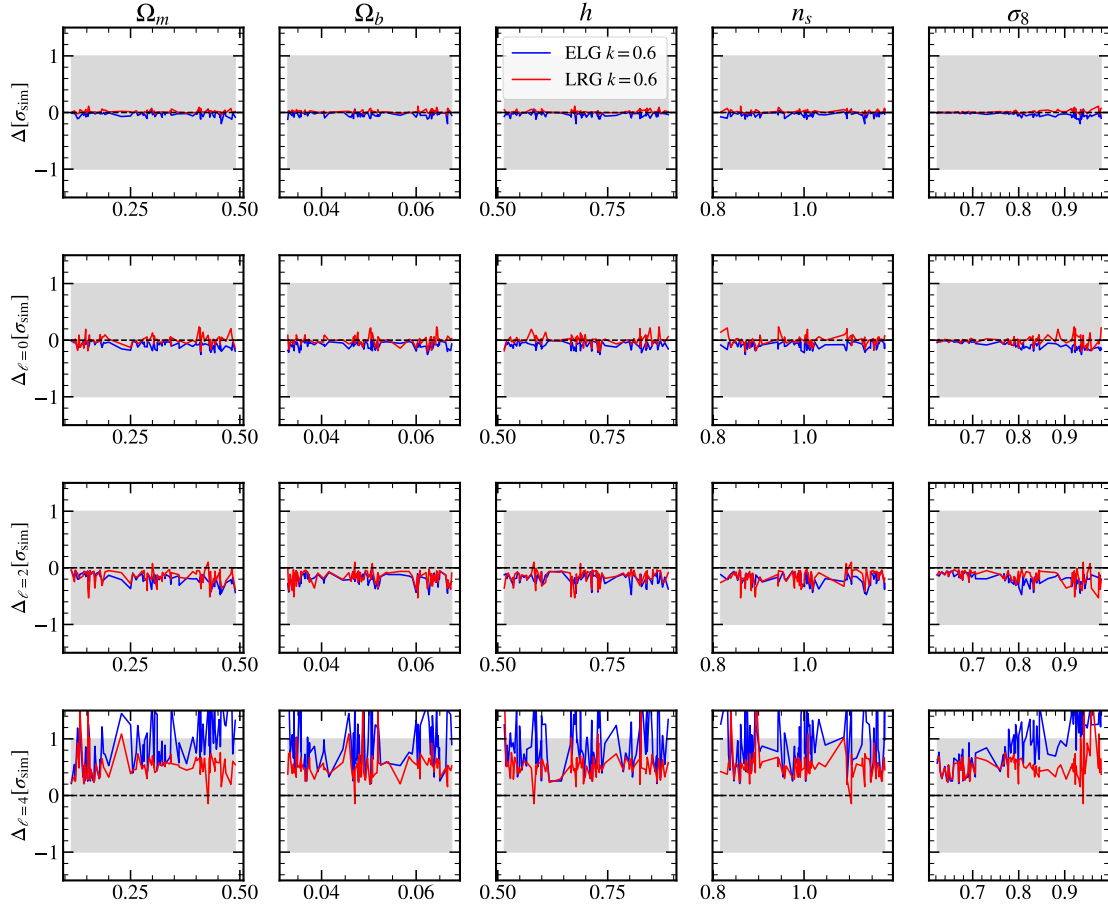


Figure 8. Difference of the power spectrum between the map2map emulation and the galaxy simulated mock in units of the simulation standard deviation at a specific wavenumber ($k = 0.6 h \text{ Mpc}^{-1}$). Each column corresponds to a different cosmological parameter, while each row represents the deviation $\Delta[\sigma_{\text{sim}}] \equiv (P_{\text{m2m}} - P_{\text{Quijote}}) / \sigma_{\text{Quijote}}$, which quantifies the difference in the 2-point statistics (in redshift or real space) normalized by the standard deviation of the Quijote simulations.

with the Lagrangian bias expansion, the hybrid bias expansion offers a general solution to model LSS tracers such as galaxies at the field level.

By comparing biased fields constructed using either simulations from the Quijote simulation suite or predictions from map2map, we were able to quantify the accuracy of our approach for the power spectrum in real and redshift space, as well as for their variance, the field statistics, and cosmological dependence.

We focused on two samples mimicking galaxies to be observed by the upcoming surveys – Emission-line galaxies with relatively modest bias parameters at $z \sim 1$ and Luminous red galaxies with larger bias parameters at somewhat lower redshifts $z \sim 0.6$.

In real space, we find that the galaxy fields predicted by our approach closely describe our simulation results on large scales. On intermediate scales, although accurate at the 1% level, there are statistically significant biases. These, however, can be almost completely absorbed by the nuisance parameters of the hybrid bias expansion that describe the stochastic component of galaxy bias.

Similarly, in redshift space, we found that our emulated results are accurate on large scales but are systematically biased for $k > 0.1 \sim 0.2 h \text{ Mpc}^{-1}$. We attribute this to an additional small-scale velocity dispersion in the map2map predictions. This likely is the result of inaccuracies in exactly detecting the boundary of haloes and their center-of-mass velocities. However, these too can be absorbed by the

nuisance parameters of the redshift-space modelling. Specifically, by the parameter that describes the intra-halo velocity dispersion of the target galaxy samples, which leads to accuracies of within 1σ down to scales of $k \sim 0.6 h \text{ Mpc}^{-1}$.

Additionally, we showed that our approach can accurately predict the variance and off-diagonal covariance terms of real and redshift space quantities. This opens up the possibility of estimating covariance matrices with very little numerical noise as our approach can deliver thousands of mock catalogues at a small computational cost.

Through tests of field-level performance, we have observed that map2map accurately reconstructs both real and redshift space fields, surpassing the anticipated noise levels present in the considered mock datasets. In particular, the accuracy extends to scales of approximately $k \sim 1 h \text{ Mpc}^{-1}$ in real space and $k \sim 0.35 h \text{ Mpc}^{-1}$ in redshift space, where the main limitation is the emulated quadrupole.

Remarkably, these outcomes persist even when varying the cosmological parameters, emphasising the suitability of our approach for precise parameter estimation at the field level. However, it is worth noting a residual dependency on σ_8 , where larger deviations are observed at higher values of this parameter. We plan to address this issue in future works.

ACKNOWLEDGEMENTS

MPI and RA would like to thank Francisco Maion for useful discussions. The authors acknowledge the support of the ERC-StG number 716151 (BACCO). MPI acknowledges the support of the “Juan de la Cierva Formación” fellowship (FJC2019-040814-I). REA acknowledges the support of the Project of excellence Prometeo/2020/085 from the Conselleria d’Innovació, Universitats, Ciència i Societat Digital de la Generalitat Valenciana, and of the project PID2021-128338NB-I00 from the Spanish Ministry of Science. This research was supported by the Munich Institute for Astro-, Particle and Bio-Physics (MIAPbP) which is funded by the Deutsche Forschungsgemeinschaft (DFG, German Research Foundation) under Germany’s Excellence Strategy – EXC-2094 – 390783311.

DATA AVAILABILITY

The data used throughout this paper is available in the following sources. The Quijote simulations are publicly available at the Quijote webpage². The hybrid model can be computed from the baccoemu code³. The map2map code with the trained weights can be downloaded from github⁴. The rest of the products will be shared upon reasonable request to the authors.

REFERENCES

- Alves de Oliveira R., Li Y., Villaescusa-Navarro F., Ho S., Spergel D. N., 2020, *Machine Learning and the Physical Sciences*, NeurIPS 2020
- Amendola L., et al., 2018, *Living Reviews in Relativity*, **21**, 2
- Balaguera-Antolínez A., et al., 2019a, *MNRAS*, **p. 2800**
- Balaguera-Antolínez A., Kitaura F.-S., Pellejero-Ibañez M., Zhao C., Abel T., 2019b, *MNRAS*, **483**, L58
- Balaguera-Antolínez A., et al., 2023, *A&A*, **673**, A130
- Banerjee A., Abel T., 2021, *MNRAS*, **500**, 5479
- Beutler F., et al., 2017, *MNRAS*, **464**, 3409
- Blake C., et al., 2010, *MNRAS*, **406**, 803
- Blot L., et al., 2019, *MNRAS*, **485**, 2806
- Boruah S. S., Rozo E., 2023, *arXiv e-prints*, **p. arXiv:2307.00070**
- Cabass G., Schmidt F., 2020, *J. Cosmology Astropart. Phys.*, **2020**, 042
- Cheng S., Ting Y.-S., Ménard B., Bruna J., 2020, *MNRAS*, **499**, 5902
- Cole S., et al., 2005, *MNRAS*, **362**, 505
- Contreras S., Angulo R. E., Zennaro M., 2021a, *MNRAS*, **504**, 5205
- Contreras S., Angulo R. E., Zennaro M., 2021b, *MNRAS*, **508**, 175
- Desjacques V., Jeong D., Schmidt F., 2018, *Phys. Rep.*, **733**, 1
- Dodelson S., Schneider M. D., 2013, *Phys. Rev. D*, **88**, 063537
- Eggemeier A., Battefeld T., Smith R. E., Niemeyer J., 2015, *MNRAS*, **453**, 797
- Feng Y., Chu M.-Y., Seljak U., McDonald P., 2016, *MNRAS*, **463**, 2273
- Grieb J. N., Sánchez A. G., Salazar-Albornoz S., Dalla Vecchia C., 2016a, *Monthly Notices of the Royal Astronomical Society*, **457**, 1577
- Grieb J. N., Sánchez A. G., Salazar-Albornoz S., Dalla Vecchia C., 2016b, *Mon. Not. Roy. Astron. Soc.*, **457**, 1577
- Hahn C., et al., 2023, *J. Cosmology Astropart. Phys.*, **2023**, 010
- He S., Li Y., Feng Y., Ho S., Ravanbakhsh S., Chen W., Póczos B., 2019, *Proceedings of the National Academy of Sciences*, **116**, 13825
- Ivanov M. M., Philcox O. H. E., Cabass G., Nishimichi T., Simonović M., Zaldarriaga M., 2023, *arXiv e-prints*, **p. arXiv:2302.04414**
- Jackson J. C., 1972, *MNRAS*, **156**, 1P

- Jamieson D., Li Y., Alves de Oliveira R., Villaescusa-Navarro F., Ho S., Spergel D. N., 2022, *arXiv e-prints*, **p. arXiv:2206.04594**
- Kaushal N., Villaescusa-Navarro F., Giusarma E., Li Y., Hawry C., Reyes M., 2022, *ApJ*, **930**, 115
- Kitaura F. S., Balaguera-Antolínez A., Sinigaglia F., Pellejero-Ibañez M., 2022, *MNRAS*, **512**, 2245
- Kokron N., DeRose J., Chen S.-F., White M., Wechsler R. H., 2021, *MNRAS*, **505**, 1422
- Kostić A., Nguyen N.-M., Schmidt F., Reinecke M., 2022, *arXiv e-prints*, **p. arXiv:2212.07875**
- Laureijs R., et al., 2011, *arXiv e-prints*, **p. arXiv:1110.3193**
- Levi M., et al., 2013, preprint, (**arXiv:1308.0847**)
- Li Y., Ni Y., Croft R. A. C., Di Matteo T., Bird S., Feng Y., 2021, *Proceedings of the National Academy of Science*, **118**, e2022038118
- Modi C., Chen S.-F., White M., 2020, *MNRAS*, **492**, 5754
- Moresco M., et al., 2022, *Living Reviews in Relativity*, **25**, 6
- Ni Y., Li Y., Lachance P., Croft R. A. C., Di Matteo T., Bird S., Feng Y., 2021, *MNRAS*, **507**, 1021
- Orsi Á. A., Angulo R. E., 2018, *MNRAS*, **475**, 2530
- Pakmor R., et al., 2022, *arXiv e-prints*, **p. arXiv:2210.10060**
- Pellejero-Ibañez M., et al., 2020, *MNRAS*, **493**, 586
- Pellejero Ibañez M., Stücker J., Angulo R. E., Zennaro M., Contreras S., Aricò G., 2022, *MNRAS*, **514**, 3993
- Pellejero-Ibañez M., et al., 2017, *Monthly Notices of the Royal Astronomical Society*, **468**, 4116
- Pellejero Ibañez M., Angulo R. E., Zennaro M., Stücker J., Contreras S., Aricò G., Maion F., 2023, *Monthly Notices of the Royal Astronomical Society*, **520**, 3725
- Perko A., Senatore L., Jennings E., Wechsler R. H., 2016, *arXiv e-prints*, **p. arXiv:1610.09321**
- Philcox O. H. E., Ivanov M. M., 2022, *Phys. Rev. D*, **105**, 043517
- Pisani A., et al., 2019, *BAAAS*, **51**, 40
- Porqueres N., Heavens A., Mortlock D., Lavaux G., Makinen T. L., 2023, *arXiv e-prints*, **p. arXiv:2304.04785**
- Pozzetti L., et al., 2016, *A&A*, **590**, A3
- Sargent W. L. W., Turner E. L., 1977, *ApJ*, **212**, L3
- Schmittfull M., Simonović M., Assassi V., Zaldarriaga M., 2019, *Phys. Rev. D*, **100**, 043514
- Sinigaglia F., Kitaura F.-S., Balaguera-Antolínez A., Nagamine K., Ata M., Shimizu I., Sánchez-Benavente M., 2021, *ApJ*, **921**, 66
- Stadler J., Schmidt F., Reinecke M., 2023, *arXiv e-prints*, **p. arXiv:2303.09876**
- Tassev S., Zaldarriaga M., Eisenstein D. J., 2013, *J. Cosmology Astropart. Phys.*, **2013**, 036
- Valogiannis G., Dvorkin C., 2022a, *Phys. Rev. D*, **105**, 103534
- Valogiannis G., Dvorkin C., 2022b, *Phys. Rev. D*, **106**, 103509
- Villaescusa-Navarro F., et al., 2020, *ApJS*, **250**, 2
- Villaescusa-Navarro F., et al., 2021, *arXiv e-prints*, **p. arXiv:2109.10360**
- Yuan S., Hadzhiyska B., Abel T., 2023, *MNRAS*, **520**, 6283
- Zennaro M., Angulo R. E., Pellejero-Ibañez M., Stücker J., Contreras S., Aricò G., 2021, *arXiv e-prints*, **p. arXiv:2101.12187**
- Zennaro M., Angulo R. E., Contreras S., Pellejero-Ibañez M., Maion F., 2022, *MNRAS*, **514**, 5443
- Zhang X., Lachance P., Ni Y., Li Y., Croft R. A., Di Matteo T., Bird S., Feng Y., 2023, *arXiv preprint arXiv:2305.12222*

APPENDIX A: REDSHIFT-SPACE OPERATORS

The accuracy of the map2map operators in redshift space is shown in Figure A1, illustrating the fractional difference observed among each of the cross-spectra. To provide clarity, the differences are presented in terms of the standard deviation measured in the Quijote realisations. The error bars represent the scatter determined from the map2map recovered spectra. Thus, a scatter closer to 1 indicates a better recovery of the diagonal terms of the covariance matrix. We explore this further in the main text.

On large scales ($k < 0.1 h \text{ Mpc}^{-1}$), the emulated and simulated

² <https://quijote-simulations.readthedocs.io/en/latest/>

³ <https://baccoemu.readthedocs.io/en/latest/>

⁴ https://github.com/dsjamieson/map2map_emu/

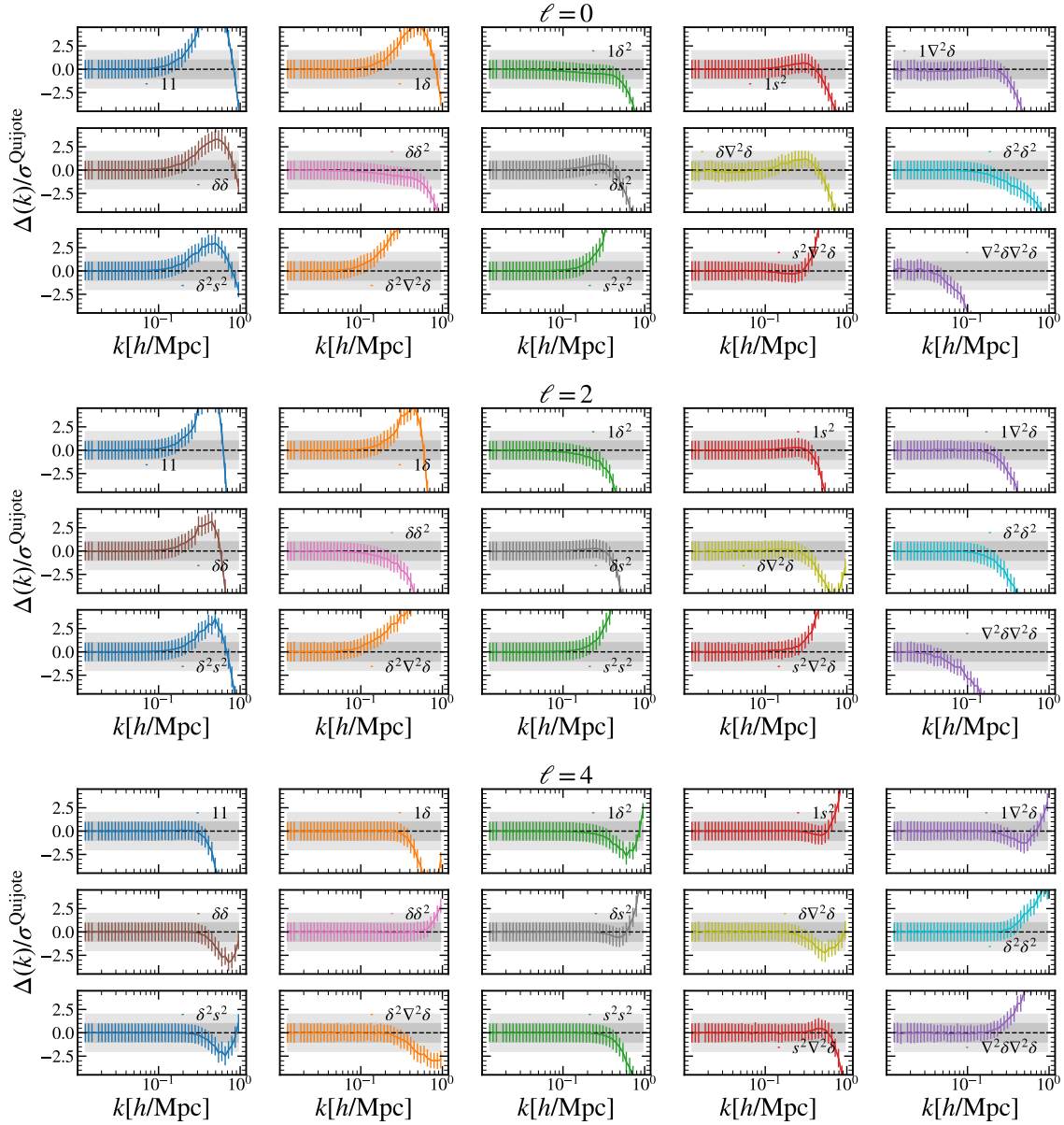


Figure A1. The figure presents the relative difference between the predictions of map2map and the measurements obtained from the Quijote suite, expressed in units of the simulation variance for a $1h^{-3}\text{Gpc}^3$ volume. Specifically, we consider the quantity $(P_{\text{m2m}}^\ell - P_{\text{Quijote}}^\ell)/\sigma_{\text{Quijote}}^\ell$, where P_{m2m}^ℓ and P_{Quijote}^ℓ represent the monopole, quadrupole, or hexadecapole power spectra in redshift space for each respective operator field advected to $z = 0$. Each panel of the figure corresponds to a different operator field, as indicated in the respective captions. The solid lines represent the average relative difference, while the vertical error bars represent the standard deviation, calculated over 100 realizations.

cross-spectra exhibit statistical compatibility. However, on smaller scales, systematic deviations are detected regardless of the multipole, with map2map either over- or under-predicting the signal by more than 3σ , depending on the specific spectra. It is worth noting that despite the presence of this bias, its magnitude remains extremely small. For example, for the P_{11} term, the bias corresponds to only 1.5% at $k = 1h\text{Mpc}^{-1}$. The overall significance and relative importance of uncertainties in each $P_{i,j}$ term depend on the specific bias parameters characterising the given galaxy sample, which is explored in this work. Our findings reveal that, with realistic bias values, these differences can be effectively absorbed through the calibration of the

model nuisance parameters, leading to results within 1σ for both the ELG and LRG samples.

This paper has been typeset from a \LaTeX file prepared by the author.